Shading correction for endoscopic images using principal color components

Article *in* International Journal of Computer Assisted Radiology and Surgery · August 2015

DOI: 10.1007/s11548-015-1273-3 · Source: PubMed

3 authors:

Tobias Bergen
Fraunhofer Institute for Integrated Circuits IIS
39 PUBLICATIONS **221** CITATIONS
SEE PROFILE

Thomas Wittenberg
Friedrich-Alexander-University of Erlangen-Nürnberg
421 PUBLICATIONS **2,332** CITATIONS
SEE PROFILE

Christian Münzenmayer
Fraunhofer Institute for Integrated Circuits IIS
98 PUBLICATIONS **460** CITATIONS
SEE PROFILE

IJCARS manuscript No.
(will be inserted by the editor)

Shading correction for endoscopic images using principal color components

Tobias Bergen · Thomas Wittenberg · Christian Münzenmayer

Received: date / Accepted: date

Abstract *Purpose* Inhomogeneous illumination often causes significant shading and vignetting effects in images captured by an endoscope. Most of the established shading correction methods are designed for gray level images. Only few papers have been published about how to compensate for shading in color images. For endoscopic images with a distinct red coloring, these methods tend to produce color artifacts.
Method A color shading correction algorithm for endoscopic images is proposed. Principal component analysis is used to calculate an appropriate estimate of the shading effect so that a one-channel shading correction can be applied without producing undesired artifacts.
Results The proposed method is compared to established YUV and HSV color conversion based approaches. It produces superior results both on simulated and on real endoscopic images. Example images of using the proposed shading correction for endoscopic image mosaicking are presented.
Conclusion A new method for shading correction is presented which is tailored to images with distinct coloring. It is beneficial for the visual impression and further image analysis tasks.

Keywords color shading correction · de-vignetting · principal component analysis · endoscopy · image stitching

1 Introduction

Inhomogeneity of illumination intensity is a common phenomenon in images captured by a camera. For many endoscopic imaging systems this effect is very distinct and shows itself as a slowly decreasing intensity from the image

T. Bergen
Fraunhofer Institute for Integrated Circuits IIS, Erlangen, Germany
E-mail: tobias.bergen@iis.fraunhofer.de

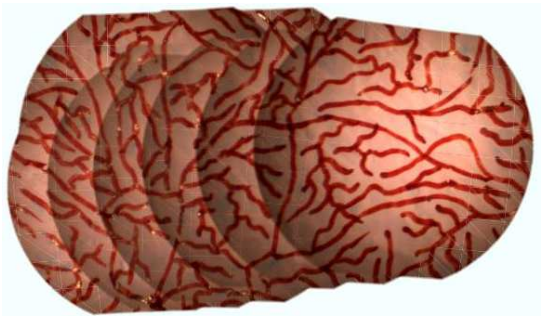

Fig. 1 Image stitching methods have been used to generate the impression of a wide field of view for endoscopic inspection of the urinary bladder. A mosaic generated from images of a bladder phantom is depicted here. Inhomogeneous illumination causes a disturbing shading effect.

center towards the edges. This effect is also known as *vignetting*. The shading effect can be caused by any imperfection of the image acquisition process, such as inhomogeneous illumination, limitations of the lens system, dirt or dust on the lens or the camera sensor. For endoscopic images, the vignetting effect is mainly due to the wide viewing angle (typically between 90°and 120°) and the fact that the light source is directed toward the center of the field of view, causing inhomogeneous illumination. Furthermore, the optical setup with a light source at the proximal end of the endoscope and usually a glass fiber cable transmission produces a small angle of illumination, which leads to the observed shading effect. While this effect is of minor importance for the human visual perception of image information, it causes difficulties for many computer vision and pattern recognition tasks, such as texture analysis for computer assisted diagnosis (CAD), image registration, image stitching, and 3D reconstruction. De-vignetting or shading correction is often a necessary pre-processing step for such algorithms to compensate for such intensity inhomogeneities. Fig. 1 depicts an example of a stitched image of a urinary bladder phantom, where a disturbing shading effect is clearly visible The image has been stitched using a method which we described earlier [1,2].

If the shading effect is mainly caused by characteristics of the imaging system that are invariant to time or camera motion, prospective shading correction can be performed as calibration step using an apriori estimate of the shading model. This usually involves the recording of test images of known objects (such as black and white reference patterns) [16]. For endoscopic applications the shading depends on both the distance and perspective alignment between the endoscope tip and the object (object-dependent shading), so that a shading correction filter cannot be kept constant, but has to be recalculated for every image. This is called retrospective shading correction and inhibits the use of known calibration images. The shading has to be derived from the current image only. In the context of endoscopic image stitching, several authors have explicitly addressed the problem of compensating vignetting effects in a dedicated pre-processing step within their stitching algorithm [6,8,15]. It

is generally assumed, that due to varying configurations between light-source and object, shading correction has to be applied retrospectively. In this paper, we will therefore address the problem of retrospective color shading correction.

For the correction of shading effects in gray-level images, several solutions have been proposed by the image processing research community since the 1990s. The underlying principles and models will be reviewed in Sec. 2. For shading in color images, very few contributions can be found in the literature. While for general color images a gray world assumption may be valid in many contexts, for endoscopy the observed images are usually dominated by red coloring due to the appearance of the interior of the human body. Priorly known solutions for color shading correction based on YUV and HSV color space conversions often cause undesired color artifacts in the context of endoscopic imaging. We therefore propose a new retrospective shading correction approach based on principal component analysis (PCA) of the RGB color space in Sec. 3 to account for this problem. The approach will be compared to the methods based on YUV and HSV color space conversions in Sec. 4. Finally, the effect of shading correction as a pre-processing step for endoscopic image mosaicking will be demonstrated.

2 Related Work

2.1 Gray Level Shading Correction

According to Tomazevic et al. [11,12], the relation of a shading-free image $U(x, y)$ and the observed image intensities $N(x, y)$ can be formulated as a general function f

$$N(x, y) = f(U(x, y)). \tag{1}$$

Thus, the task of retrospective shading correction is described by finding the inverse function f^{-1}

$$U(x, y) = f^{-1}(N(x, y)). \tag{2}$$

While f may in general model a complex relation between $U(x, y)$ and $N(x, y)$, a linear approximation of f is commonly used [16,12] to model the variation of image intensity caused by shading effects, leading to

$$N(x, y) = U(x, y)S_M(x, y) + S_A(x, y), \tag{3}$$

where $S_M(x, y)$ models a multiplicative and $S_A(x, y)$ an additive shading component. Since retrospective shading correction inhibits the use of calibration images, $S_M(x, y)$ and $S_A(x, y)$ have to be estimated solely from the observed image $N(x, y)$. Several approaches have been proposed to estimate the shading within the image.

The *linear filter approach* is based on the assumption that the shading is only present in the low-frequency domain of the image spectrum, so it can

be recovered with a low-pass filter (LPF). Linear filtering assumes an additive shading model and is able to give an estimate $\hat{S}_A(x, y)$ of the additive component [9,11,12,16]:

$$\hat{S}_A(x, y) = \mathrm{LPF}\{N(x, y)\} + C_A, \tag{4}$$

where C_A represents a constant needed to restore a desired gray level (e. g. the mean value of the shading estimate).

Instead of estimating the additive shading component, *homomorphic filtering* estimates the multiplicative component by performing the low-pass filter operation on the logarithm of the image

$$\hat{S}_M(x, y) = \exp\left(\mathrm{LPF}\{\log(N(x, y))\}\right) \cdot C_M. \tag{5}$$

C_M represents a multiplicative constant to restore an adequate gray level.

Further methods have been proposed to estimate either one of the shading components or both of them. *Morphological filtering* can be used to produce a smoothed version of the image if the size of objects in the image is known [16]. Similarly to the linear filter approach, the smoothed image can be used to estimate either $\hat{S}_A(x, y)$ or $\hat{S}_M(x, y)$. Alternatively, the shading component can be estimated by fitting a model to selected points of the image. Commonly, polynomials of second degree are used as shading models [11,12]. Based on the assumption that shading increases the level of uncertainty in the observed image, Likar et al. [7] combined polynomial fitting with an entropy minimization step to generate an estimate of the unshaded image $\hat{U}(x, y)$.

2.2 Color Shading Correction

Literature about shading correction of color images is very sparse. Two general approaches can be identified, which we will call *intra-plane* shading correction and *intensity-based* shading correction. Let the image I be represented as a three-channel RGB-image $I^{RGB} = \{I^R, I^G, I^B\}$.

Intra-plane approaches apply gray level shading correction methods independently to each of the three planes of the color image. This is a straightforward extension and has been proposed by Derganc et al. [5] who extended the entropy-minimization method of Likar et al. [7] to color images for the purpose of robust color image segmentation.

Münzenmayer et al. [9] argue that since an RGB image encodes both intensity and chromaticity in all channels, the intra-plane filtering approach may undesirably influence color information. They propose an intensity-based method which first separates intensity and chromaticity information to subsequently correct only image intensity. They chose the YUV color space [10] to extract the luminance Y from the image and apply binomial gray level filtering to estimate $\hat{S}_A(x, y)$ and correct the image without modifying the UV-channels. After this modification the image is converted back into the RGB color space. Obviously, any of the gray level algorithms could be applied

in such fashion. Cavalcanti et al. [3] follow a very similar approach and use the HSV color space [10] to get an estimate of the image intensity (V) and model the shading with a quadric function.

While these intensity-based methods show great potential for efficient retrospective shading correction of color images, they are not without problems. The assumption is made, that the conversion to one of the common color spaces reliably separates intensity and chromaticity information and that only the intensity channel is affected by the shading. Although this may be a good assumption for a general scenario (presumably a gray world), experiments have shown that the produced results are not satisfactory for endoscopic images which show a dominant red coloring. Both YUV and HSV smoothing methods produce undesirable color artifacts.

2.3 Intensity-based shading correction of endoscopic images

Experiments with endoscopic images reveal the problem involved with the proposed color space conversions YUV and HSV. Fig. 2 (a)-(c) show an endoscopic image of the interior wall of the human bladder together with the respective YUV and HSV corrected images. The linear filter approach has been used for these experiments. Notice, how the shading correction successfully equalizes the observed level of brightness across the image (most noticeable in the bottom left corner), but at the cost of a gray coloring in the case of YUV conversion and an intense red coloring in the case of HSV conversion.

These color artifacts indicate that the color conversions used are not adequate to isolate the shading effect into one color channel (Y or V, respectively). This observation is supported by Fig. 2 (d)-(f). A profile is depicted for the three channels of the YUV and HSV converted background estimations of one row of the bladder image. Ideally, only one color component should show any variation from left to right. It can be observed that in the case of HSV conversion the shading influences the V-component as expected but also the saturation value changes significantly. Using YUV conversion, the U and V channels are quite stable but there is still noticeable variance towards the image edges. This observation constitutes the color artifacts perceived above and motives using principal component analysis (PCA) to identify a suitable color space transformation. The proposed method is motivated by a previous paper by Cheng and Hsia [4] who proposed PCA for different color image processing tasks such as color edge detection, color image sharpening, and color image compression.

3 Color shading correction with principal color components

3.1 Principal Color Components (PCC)

Motivated by the observation in the previous section, a new approach for color shading correction based on principal components is proposed. Principal com-

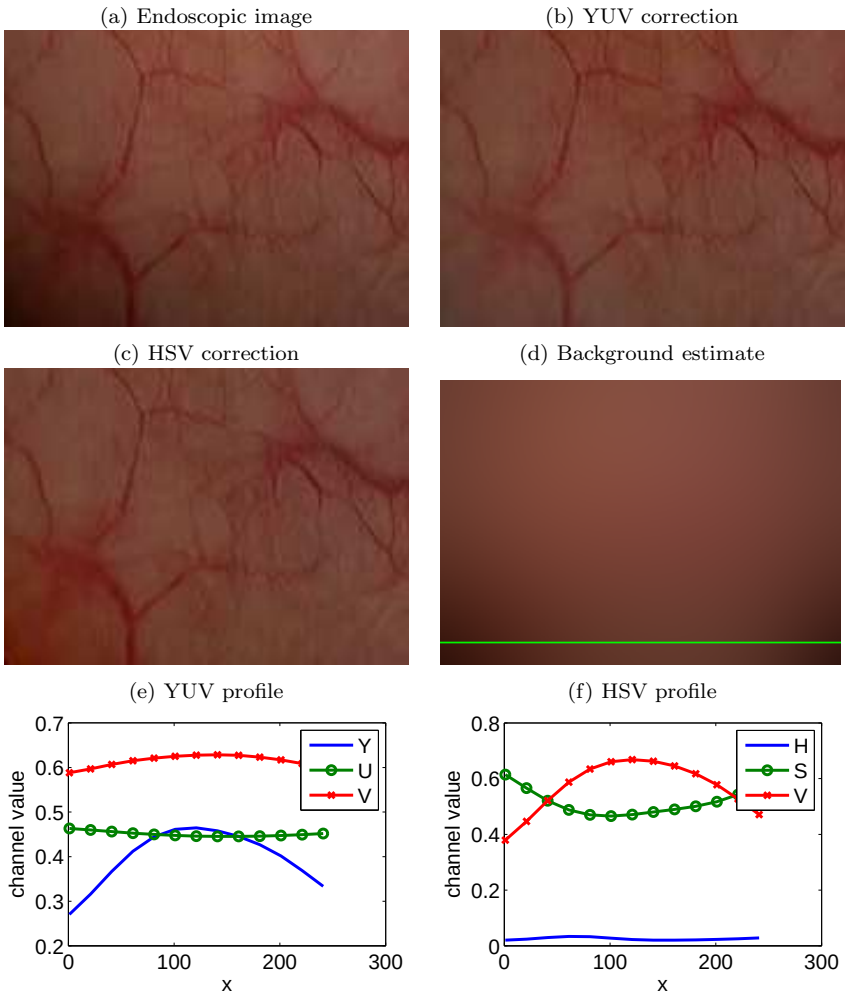

Fig. 2 (a) An endoscopic image of the human bladder with shading effect. Mind the bottom left corner of each image. (b) Corrected image using the YUV color space. Notice the gray color at the bottom left corner. (c) Corrected image using the HSV color space. Notice the intense red color at the bottom left corner. The diagrams (e) and (f) show profiles of one line of the bladder image background estimate (d) for the YUV (e) and HSV conversions (f). For both conversions, the shading affects more than one component.

ponent analysis (PCA) converts a set of observed pixel values in RGB color space into a set of linearly uncorrelated color components, which we call *principal color components* (PCC). The three components are called C_1, C_2, C_3. If PCA is applied to the shading estimate in RGB color space, the first principal component has maximal variance and optimally encodes the image intensity and thus the shading effect in one channel. The variances of the second and third components provide a measure of how well the shading effect is rep-

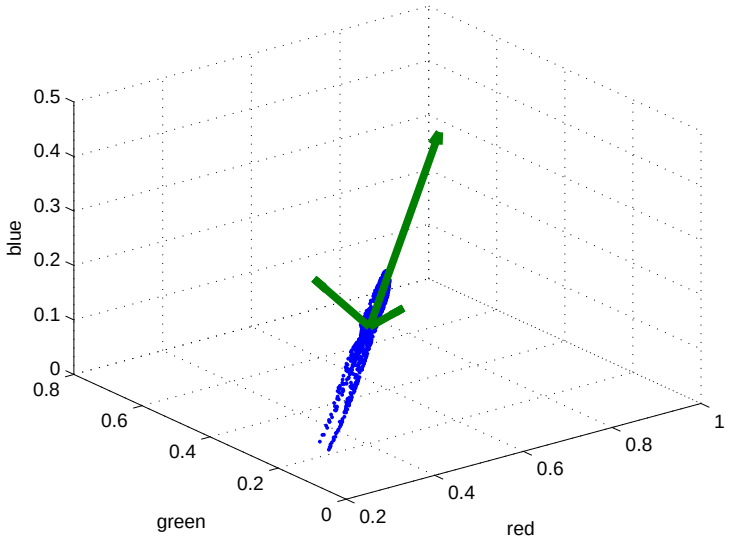

Fig. 3 Visualization of RGB pixel values of the estimated shading of an endoscopic bladder image. The principal components are indicated as arrows.

resented by the first component. To provide a visual impression of shading linearity in endoscopic images, Fig. 3 depicts the RGB values of the estimated shading image (smoothed version of the input image).

An experiment was conducted to evaluate the linearity of the shading effect in the RGB color space. 525 endoscopic images with visible shading were randomly selected from a large database of different endoscopic procedures (including cystoscopy, colonoscopy, gastroscopy, and neurosurgery). For each image a score of linearity was calculated. Identifying the principal color components using singular value decomposition yields the principal axes as well as the corresponding singular values. The latter are proportional to the standard deviations of the given data along the principal axes [14]. Thus, the ratio of variance along the first principal axis to the total variance gives a measure of linearity. Let $\sigma_{i1}, \sigma_{i2}, \sigma_{i3}$ denote the singular values of the i-th image. Then

$$l_i = \frac{\sigma_{i1}^2}{\sum_{j=1}^{3} \sigma_{ij}^2} \tag{6}$$

defines the score of linearity l of the i-th image with $l = 1$ for perfect linearity. The mean linearity score over all 525 images was 0.992 with a standard deviation of 0.01. It can be concluded, that a linear model is adequate to describe the distribution of the intensity values (and therefore the shading) in the RGB color space and that the PCC conversion is able to aggregate the shading effect within the first component. The ratio of variances has also been calculated for all images after conversion to the YUV and HSV color space, respectively.

Table 1 Ratio of variances of pixel values after applying PCC, YUV, and HSV color transforms. A value of 1 indicates that the pixel value variance is concentrated in one channel.

		Mean	Std. dev.		Mean	Std. dev.		Mean	Std. dev.
PCC	C_1	0.992	(±0.01)	C_2	0.008	(±0.01)	C_3	0.0	(±0.0)
YUV	Y	0.919	(±0.064)	U	0.02	(±0.017)	V	0.062	(±0.05)
HSV	H	0.181	(±0.308)	S	0.157	(±0.147)	V	0.662	(±0.285)

Table 1 summarizes the results. It can be observed that the Y component of the YUV color space only aggregates 91.9% of the total variance and the V component of the HSV color space only aggregates 66.2%, indicating that the shading effect is not well separated by these conversions.

3.2 PCC Shading Correction

The proposed PCC shading correction adapts the linear filtering approach described by Equ. 4 for color images. A low-pass filter is used to get an estimate of the additive shading component $\hat{S}_A^{RGB}(x, y)$ (which will also be called background image) in the RGB color space. The low-pass filter can be realized by a Gaussian smoothing filter or an efficient average filter based on integral images, which is the preferred method since kernel sizes tend to be large. For the experiments presented in Sec. 4 an average filter based on integral images is used. For an image with dimensions $M \times N$, the filter mask is chosen to be of size $\frac{(M+N)}{8}$. From the set of background pixels the principal color components are extracted using singular value decomposition. The singular value decomposition decomposes the data matrix of pixel colors X into $X = U\Sigma V$. Every row of X contains the red, green, and blue values of one pixel, shifted to form a zero-mean distribution. The resulting matrix V is a 3×3 orthonormal matrix which describes the linear transform (a 3D rotation) to align the RGB color space with the principal axes. Consequently, the conversion of an image pixel $I^{RGB}(x, y)$ from RGB to PCC color space is a simple matrix multiplication

$$I^{PCC}(x, y) = I^{RGB}(x, y)V. \tag{7}$$

Fig. 4 depicts the work-flow of the proposed method. The calculation of the conversion matrix V can be implemented as a training step which is not performed on every single image of an image sequence if the images can be expected to have a similar coloring. Instead, a training image set can be defined or the training can be implemented "on-the-fly" by using every n-th image of an image sequence to calculate an average matrix V. Nonetheless, two suggestions are made to efficiently implement the training process so that it should be possible to repeat it for every single image even in a real-time scenario. First, the smoothing operation should be implemented using efficient averaging, based on integral images [13]. Second, the data matrix X does not need to contain every single pixel of the image. A (random) subset of pixels evenly

distributed over the image should suffice to generate a decent estimate of the principal axes. For the experiments presented, 64 samples per image dimension have been used, resulting in 4096 pixel values. Since integral image smoothing allows to efficiently calculate filter responses at these distinct pixel positions, the computational load is very low compared to conventional Gaussian filtering of a three-channel image. We measured a mean total processing time of 25.6 ms (including PCA for every frame) for images of size 704×576, which is sufficient to process frames at the typical rate of 30 frames per second. The PCA calculation took about 3.2 ms on average in our experiments.

Once the image has been transformed to its principal components, any one-channel shading correction can be applied to the image consisting of the first component. For our experiments, we applied the linear filtering approach [12]. The extension of this method to color images using a YUV color space conversion has been described by Münzenmayer et al. [9]. Analogously, the proposed PCC conversion is used here. Assume that the transformation matrix V has been calculated as described above. Then an input image with shading $N^{RGB}(x, y)$ is converted to its PCC representation using Equ. 7. The first component $N^{C_1}(x, y)$ is corrected by calculating a gray level shading image $\hat{S}_A^{C_1}(x, y)$ using Equ. 4 and the shading-free estimate is given by

$$\hat{U}^{C_1}(x, y) = N^{C_1}(x, y) - \hat{S}_A^{C_1}(x, y). \tag{8}$$

The constant C_A in Equ. 4 serves to restore a suitable gray level. The mean value or the maximum value of the shading estimate $\hat{S}_A^{C_1}(x, y)$ have shown to be adequate choices for C_A. For our experiments, we used the maximum value. The other two PCC image channels are left unchanged

$$\hat{U}^{C_2C_3}(x, y) = N^{C_2C_3}(x, y). \tag{9}$$

Finally, the inverse color conversion

$$\hat{U}^{RGB}(x, y) = \hat{U}^{PCC}V^T \tag{10}$$

is applied (with V^T being the transposed conversion matrix) to yield the shading corrected RGB image.

4 Results

To evaluate the proposed PCC color shading correction method it is compared to the corresponding methods using YUV and HSV color space conversion both on simulated images with known ground truth as well as real images captured during endoscopic procedures.

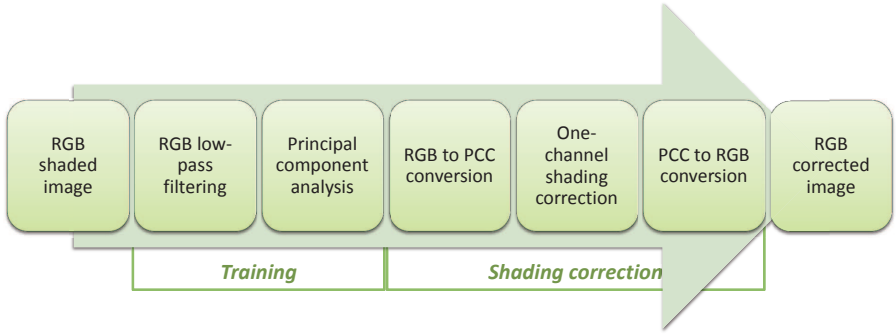

Fig. 4 The work-flow of PCC shading correction.

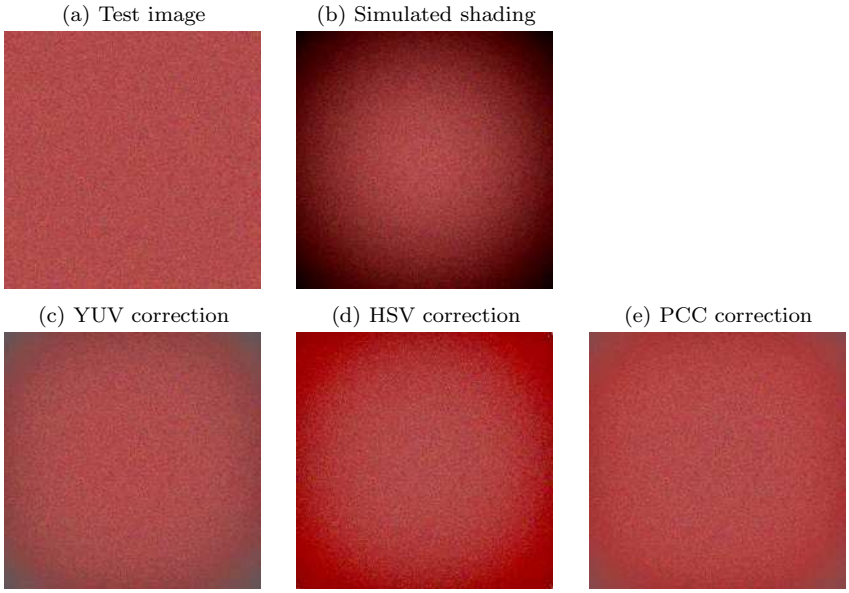

Fig. 5 A test image generated from normal distributed noise with artificial shading (with $s_m = 0.4$ and $s_a = 0.4$). Linear shading correction is applied using different color space conversions. PCC produces the least color artifacts.

4.1 Simulated shading

A quantitative comparison of the presented color space conversion is performed by simulating the shading effect on a synthetic image. The test image $U(x, y)$ is generated as a noise image with normal distribution with standard deviation $\sigma = 0.05$ for all three RGB color components (with values in the interval $[0, 1]$), added to a constant color value of $(R, G, B) = (0.7, 0.3, 0.3)$ (see Fig. 5 (a))

$$U(x, y) = 0.05 \cdot \mathcal{N}(0, 1) + (0.7, 0.3, 0.3)^T. \tag{11}$$

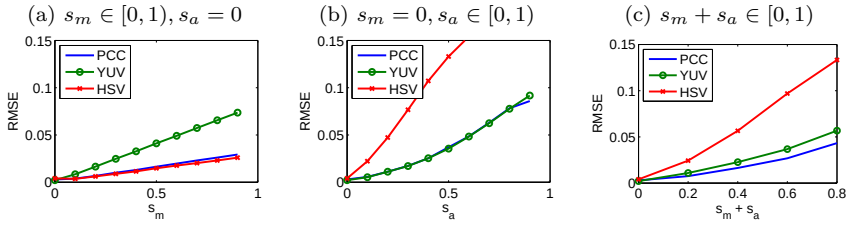

Fig. 6 For different combinations of artificial multiplicative and additive shading the root mean square error (RMSE) after correction is measured. For all cases the PCC color conversion shows the best or close to the best performance.

Shading is simulated according to the linear model (see Equ. 3) with a multiplicative shading component $S_M(x,y)$ and an additive shading component $S_A(x,y)$. Both components are defined in terms of a distance function $D(x,y)$ with a value of 1 at the image center and decreasing values towards the edges

$$D(x,y) = 1 - \frac{(x - w/2)^2 + (y - h/2)^2}{(w/2)^2 + (h/2)^2} \tag{12}$$

to simulate the vignetting effect often observed in endoscopic images (with w and h being the image width and height, respectively). The effect of the two shading components is steerable by two weighting parameters s_m and s_a. The shaded image $N(x,y)$ is defined as

$$N^i(x,y) = U^i(x,y) \cdot \left(s_m D(x,y) + (1 - s_m) + s_a(D(x,y) - 1)\right), i \in \{R,G,B\}. \tag{13}$$

An example with $s_m = 0.4$ and $s_a = 0.4$ is shown in Fig. 5 (b). Fig. 5 (c)-(e) show the corrected images $\hat{U}(x,y)$ using YUV, HSV, and PCC color conversions. As pointed out in Sec. 2.3 the YUV conversion tends to create a gray coloring, and HSV conversion overestimates the color saturation, while PCC conversion leads to the best visual result.

To quantify this impression, the *root mean square error* (RMSE) of $\hat{U}(x,y)$ with regard to the original test image $U(x,y)$ was measured for a range of parameter values for s_m and s_a. Both parameters were varied between 0 and 1 (with $s_m + s_a < 1$). Fig. 6 depicts the results. Interestingly, the type of shading (multiplicative or additive) greatly influences the performances of the YUV and HSV conversion based correction methods. For solely multiplicative shading, the HSV conversion performs well while the YUV conversion produces significantly larger errors. For solely additive shading, this observation is reversed. The PCC conversion in both cases shows the best or almost best performance, especially if both shading components are pronounced.

4.2 Shading correction of endoscopic images

Endoscopic images often suffer from intensive shading effects, mainly caused by inhomogeneous illumination. To give a visual impression of the performance of

the different shading correction methods, Fig. 7 depicts an example image with clearly visible shading and the corrected images using YUV, HSV, and PCC conversion. Since there is no ground truth with homogeneous illumination available for images acquired during endoscopic inspections, the quality of the results can only be assessed visually. As with the simulated images, the YUV correction tends to shift the dark regions towards a grayish color, while HSV correction over-saturates these regions. The PCC correction produces the least pronounced color artifacts. This is the desired effect for further image processing, such as image stitching. It is, of course, possible that surgeons might prefer a different result, such as the HSV corrected image (which is more saturated), or even the original image, since the shading may give a visual clue about the geometrical structure of the scene.

Fig. 8 shows further examples of the effect of PCC correction, applied to images from different endoscopic procedures (cystoscopy, bronchoscopy, and colonoscopy). The examples from bronchoscopy and colonoscopy show tissue lesions. Note, that the PCC correction process does not cause any perceptible modification of the coloring of the relevant structures.

Effective shading correction is of special interest if the images are to be processed further. When calculating panorama images by means of image stitching algorithms intensive shading causes visible seams between the single images. Blending methods can be applied to reduce this effect retrospectively, but a reduction of the shading as a pre-processing step is desirable to facilitate the further processing. A panorama image was calculated from a recorded sequence of images of a bladder phantom using the proposed shading correction as a pre-processing step. Fig. 9 shows the results. The PCC conversion based correction method was able to reduce the shading effect without producing any visible color artifacts.

5 Conclusion

In many endoscopic applications an undesired shading effect makes further image processing and analysis difficult. The correction of shading effects in endoscopic color images has been addressed in this paper. A new approach based on principal component analysis has been presented to find an effective color space conversion, upon which established gray level shading correction algorithms are applied. The method can be implemented very efficiently to make it suitable for real time applications. The proposed color conversion using principal color components (PCC) has been compared to YUV and HSV color representations and proved to be very effective.

A characteristic of endoscopic images is that they have a dominant red color and do not adhere to the well-known gray-world assumption, where all colors are equally present. The PCC method detects this dominant color in the estimated shading image and compensates shading along this axis. A drawback of this method may occur if different very distinct colors are present in the low-frequency components of the image and disturb the shading estima-

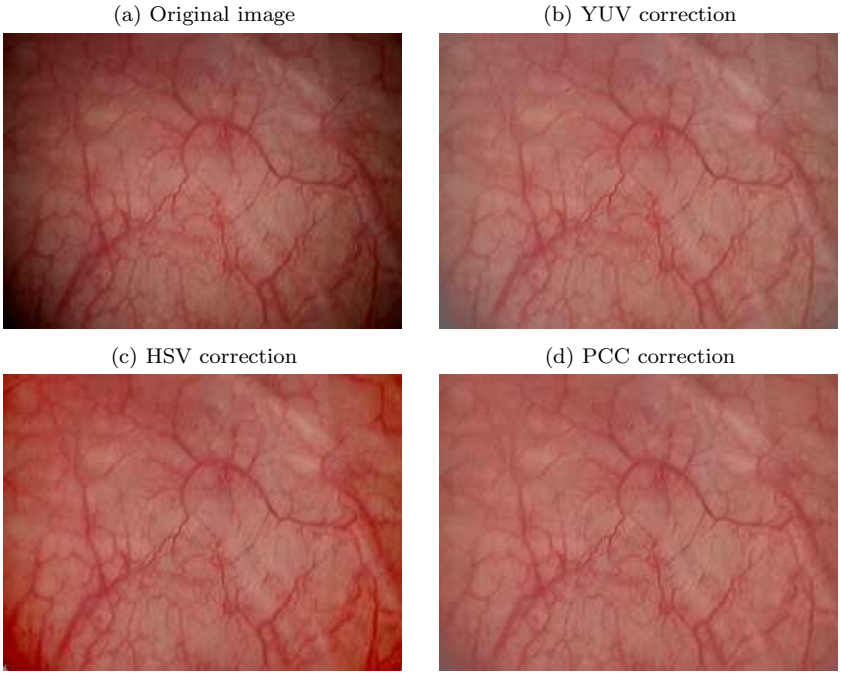

Fig. 7 The described YUV, HSV, and PCC shading correction methods have been applied to an endoscopic image of the urinary bladder. The shading effect is clearly visible in the original image (a). YUV correction (b) and HSV correction (c) produce stronger color artifacts than the PCC correction algorithm (d).

tion. Then the PCC correction moves dark pixels towards the wrong direction in color space and produces color artifacts. For YUV correction, this is the observed effect, because the YUV color conversion assumes that all shading is represented by the Y-channel, which encodes gray. Consequently, shaded image regions are brightened assuming a gray coloring, which leads to the undesired effect of gray regions in the endoscopic images. The occurrence of very distinct colors at low frequencies is very unlikely in endoscopic images, since relevant structures like lesions, tumors, or foreign objects most likely appear well-lit and in higher frequency components and do not form part of the a dark background region. Thus, no such color artifacts have been observed within the images investigated for the evaluation of the proposed method.

The proposed method has been evaluated using simulated images and real endoscopic images. The effect of shading correction was well observed when applied in the context of endoscopic image stitching. In the future, this application will be further addressed with the goal to quantitatively evaluate image mosaics in relation to the shading correction algorithm used as a preprocessing step. Also, the effect of the shading correction for the purpose of 3D reconstruction from endoscopic image sequences will be addressed in future work.

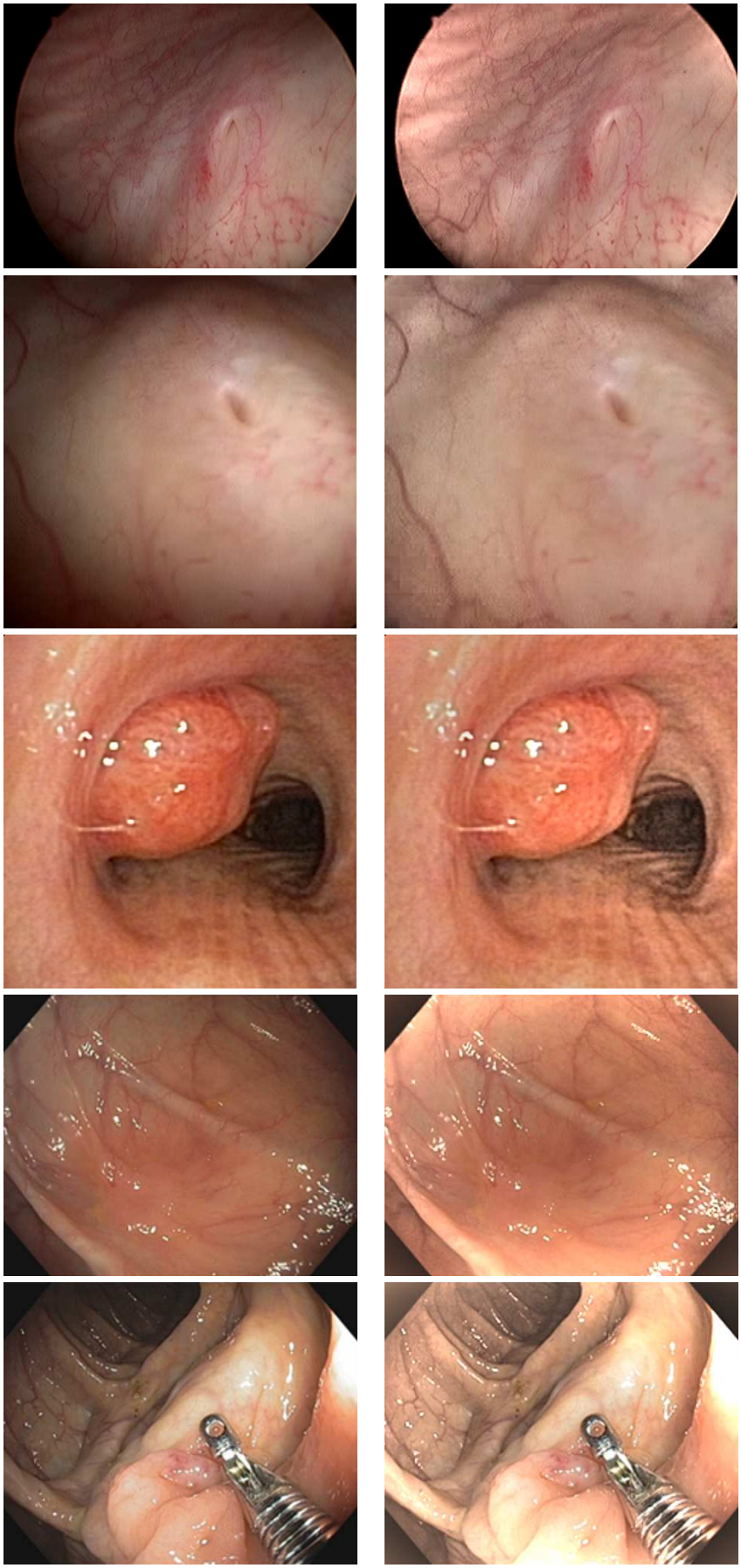

Fig. 8 A selection of endoscopic images captured different procedures: cystoscopy (rows 1 and 2), bronchosopy (row 3), colonoscopy (rows 4 and 5). The original image is depicted on the left hand side, the PCC corrected image on the right hand side.

(a) Without correction (b) PCC correction

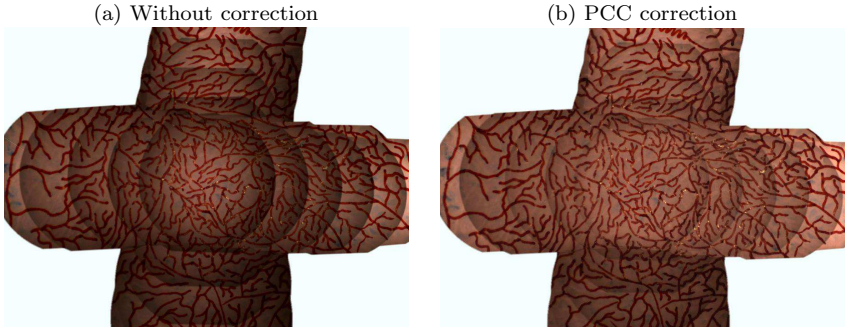

Fig. 9 An image sequence recorded from a bladder phantom has been stitched to generate a broader view field of the object. Shading effects are clearly visible in this application (a). The PCC correction (b) was able to reduce this effect without producing any visible color artifact.

Tobias Bergen, Thomas Wittenberg, and Christian Münzenmayer declare that they have no conflict of interest.

References

1. Bergen, T., Nowack, S., Münzenmayer, C., Wittenberg, T.: A hybrid tracking approach for endoscopic real-time panorama imaging. Int J CARS (Vol 8, Suppl. 1, 2013), 352–354 (2013)
2. Bergen, T., Wittenberg, T., Münzenmayer, C., Chen, C.C.G., Hager, G.D.: A graph-based approach for local and global panorama imaging in cystoscopy. In: Proc. of SPIE Vol, vol. 8671, pp. 86,711K–1 (2013)
3. Cavalcanti, P.G., Scharcanski, J.: Shading correction in human skin color images. In: Image and Video Processing: An Introductory Guide. iConcept Press, USA (2013)
4. Cheng, S.C., Hsia, S.C.: Fast algorithms for color image processing by principal component analysis. Journal of Visual Communication and Image Representation **14**(2), 184–203 (2003). DOI 10.1016/S1047-3203(03)00024-5
5. Derganc, J., Likar, B., Pernus, F.: Shading correction and segmentation of color images. In: Proceedings of the 2nd International Symposium on Image and Signal Processing and Analysis, 2001. ISPA 2001, pp. 345–350 (2001). DOI 10.1109/ISPA.2001.938653
6. Hernandez-Mier, Y., Blondel, W., Daul, C., Wolf, D., Guillemin, F.: Fast construction of panoramic images for cystoscopic exploration. Computerized Medical Imaging and Graphics **34**(7), 579–592 (2010)
7. Likar, Maintz, Viergever, Pernuš: Retrospective shading correction based on entropy minimization. Journal of Microscopy **197**(3), 285–295 (2000). DOI 10.1046/j.1365-2818.2000.00669.x
8. Miranda-Luna, R., Hernandez-Mier, Y., Daul, C., Blondel, W., Wolf, D.: Mosaicing of medical video-endoscopic images: data quality improvement and algorithm testing. In: 1st International Conference on Electrical and Electronics Engineering, 2004. (ICEEE), pp. 530–535 (2004). DOI 10.1109/ICEEE.2004.1433942
9. Münzenmayer, C., Naujokat, F., Mühldorfer, S., Wittenberg, T.: Enhancing texture analysis by color shading correction. In: 9. Workshop Farbbildverarbeitung. Zentrum für Bild-und Signalverarbeitung eV,(Ilmenau) (2003)
10. Plataniotis, P.D.K.N., Venetsanopoulos, P.A.N.: Color spaces. In: Color Image Processing and Applications, Digital Signal Processing, pp. 1–49. Springer Berlin Heidelberg (2000)

11. Tomazevic, D., Likar, B., Pernus, F.: A comparison of retrospective shading correction techniques. In: 15th International Conference on Pattern Recognition, 2000. Proceedings, vol. 3, pp. 564–567 vol.3 (2000). DOI 10.1109/ICPR.2000.903608
12. Tomaževič, D., Likar, B., Pernuš, F.: Comparative evaluation of retrospective shading correction methods. Journal of Microscopy **208**(3), 212–223 (2002). DOI 10.1046/j.1365-2818.2002.01079.x
13. Viola, P., Jones, M.: Rapid object detection using a boosted cascade of simple features. In: Proceedings of the 2001 IEEE Computer Society Conference on Computer Vision and Pattern Recognition, 2001. CVPR 2001, vol. 1, pp. I–511–I–518 vol.1 (2001). DOI 10.1109/CVPR.2001.990517
14. Wall, M.E., Rechtsteiner, A., Rocha, L.M.: Singular value decomposition and principal component analysis. In: D.P. Berrar, W. Dubitzky, M. Granzow (eds.) A Practical Approach to Microarray Data Analysis, pp. 91–109. Springer US (2003)
15. Weibel, T., Daul, C., Wolf, D., Rösch, R., Guillemin, F.: Graph based construction of textured large field of view mosaics for bladder cancer diagnosis. Pattern Recognition **45**(12), 4138 – 4150 (2012). DOI 10.1016/j.patcog.2012.05.023
16. Young, I.T., Gerbrands, J.J., Van Vliet, L.J.: Fundamentals of image processing. Delft University of Technology Delft, The Netherlands (1998)